Satellite Precipitation–based Extreme Event Detection for Flood Index Insurance

Annibale Vecere [1], Mario Martina [1], Ricardo Monteiro [1], and Carmine Galasso [1,2]

[1]University School for Advanced Studies IUSS Pavia, Pavia, Italy
[2]Dept. of Civil, Environmental & Geomatic Engineering, Univ. College London, London, United Kingdom

Correspondence to: Annibale Vecere (annibale.vecere@iusspavia.com)

Abstract. This paper introduces a novel Satellite Precipitation-based Extreme Event Detection (SPEED) model to effectively support parametric or index insurance products specifically designed to cover flood risk. Such financial instruments are intended to promote fast payouts in the aftermath of a disastrous event. They leverage on measured hazard parameters, gathered immediately after the event and defined as the trigger(s), which are used to identify such hazardous events and estimate their resulting consequences in terms of physical damage and losses.

This paper addresses the first step of such a modeling approach, the detection of a flood event, which plays an important role in the overall methodology, determining its performance in terms of false and missed detections. Different types of triggers for identifying flood events, based on satellite precipitation estimates, are investigated, and the overall model performance is assessed for a case-study country (the Philippines). A statistical procedure for selecting the optimal configuration of model parameters is presented. Such an optimal configuration minimizes the so-called basis risk, here defined in terms of the mismatch between modeled and actual events. Finally, the accuracy of the proposed approach in terms of event localization is investigated by subdividing the case-study country into three main areas, corresponding to the coarsest administrative levels, and assessing the model's capability to capture events in each considered area.

The results from this study confirm that the proposed SPEED model can be effectively used as an input for parametric insurance products, given its ability to identify hazardous events correctly.

Keywords: flood risk; parametric insurance; rapid loss estimation models; satellite precipitation estimates.

1 Introduction

The 2018 *World Disasters Report* by the International Federation of Red Cross (Fisher et al., 2018) reported 3751 natural-hazard events affecting more than 2Bn people and causing $1.658Tr worth (physical) damage in the last decade. Population increase (and consequently of exposure), as well as climate-change effects, will most likely exacerbate these figures in the near future. More effective and dynamic financial tools are required to improve rapid response and recovery in the aftermath of a disaster and to sustain preparedness further in such a context. Specifically, *ex-ante* funding mechanisms are needed to both effectively meet post-disaster needs and support disaster risk management (DRM) initiatives (Cummins & Mahul, 2009).

Recently, new insurance and/or financial strategies have been proposed to ensure pre-determined funds are available before losses are actually incurred. In this context, parametric or index insurance is playing a relevant role with respect to conventional insurance products aimed at indemnifying suffered losses. This is mainly due to parametric products' inherent ability to provide fast payouts and their cost efficiency, making them appealing to all parties involved. Payments associated with parametric coverages generally depend upon environmental variables, which are also defined as triggers, such as cumulated precipitation, earthquake magnitude, or wind speed, typically measured at the closest recording stations to a given target site (Ibarra, 2012). The payout can be based on the occurrence of a specific event with certain characteristics (e.g., earthquake exceeding a given magnitude within a pre-defined geographical area) or computed through an index defined as a function of the trigger observed values. Parametric insurance products are intended to provide cash flow to supplement foregone revenue and finance emergency response and disaster recovery. An automatic trigger can also reduce administrative costs for the insurer by eliminating the need for time-consuming/expensive field-based damage surveys. Because of the reduction in administrative costs, premiums may also be lowered, and, in turn, products made more affordable to end users. Additionally, the use of objective, measurable and accurate triggers can prevent moral hazards, i.e., when behaviors of insurance policyholders can influence the extent of damage that qualifies for insurance payouts. Nevertheless, parametric insurance is intrinsically subjected to the so-called basis risk, defined as the risk that the payments do not correspond to the occurrence of an actual event or, alternatively, that the actual losses do not match the pre-determined payout (Albertini & Barrieu, 2009).

In the last decade, parametric or index insurance received increasing attention in the context of climate risk mitigation, especially in countries with low financial capacity, which are often disproportionately affected by natural hazards. In such areas of the world, the introduction of this type of insurance can contribute to sustainable development, and its potential has been investigated in several projects worldwide. Index insurance can be used to cover a variety of hazards. However, the present study focuses on flood risk and, more specifically, on identifying events that can trigger the payout of the associated parametric coverage.

Several examples of index-based insurance to provide weather insurance for local farmers can be found in Africa, such as the National Drought Insurance for Malawi (Syroka & Nucifora, 2010) and the 'Using Satellites to Make Index Insurance Scalable' project in Ethiopia (Stanimirova et al., 2013). A similar index-insurance program has been developed in Mexico by Agroasemex (Hazell et al., 2010), the state reinsurance company, to cover crops both from excess and lack of rainfall. Two notable examples of index-based insurance products are the Caribbean Catastrophe Risk Insurance Facility (CCRIF) (CCRIF SPC, 2018), which is the first multinational index-insurance scheme to cover a series of countries within the Caribbean region against earthquakes, hurricanes, and excess of rainfall; and the index-based livestock insurance program in Mongolia, which represented one of the first examples of agriculture insurance program implemented through a country-wide agricultural risk management approach (Mahul & Skees, 2007). Parametric coverages are also gaining increasing attention both for individuals and private companies, ranging from Small and Medium Enterprises (SME) to Corporates, to cover a protection gap, as well as replacing inefficient products or introducing new products in very diverse business sectors ranging from energy to travel and leisure, but also event organization, transportation and retail (Foucart, 2013).

The "core" component of a parametric insurance scheme is an underlying methodology able to (1) detect an event causing losses (a loss event, hereinafter) based on objective criteria (i.e., the exceedance of a pre-defined threshold on a given environmental or modeled variable, that is the trigger defined above); and (2) estimate the resulting loss by means, usually, of a simplified loss model relying on an index that is a proxy of the actual loss (ASEAN, GFDRR, & UNISDR, 2012). Such a loss index is the input variable of a payout function conventionally agreed within the policy contract together with other coefficients determining the payout rule. As time is a critical variable in parametric insurance, these products' underlying methodology/models need to identify a disaster event and, possibly, estimate the associated losses promptly. Hence, they are also referred to as near real-time loss estimation models. As mentioned above, this study addresses the first component of near real-time loss estimation models (i.e., event identification – point (1) above); it proposes a modeling approach relying on satellite-based precipitation estimates as the environmental variable (trigger) to identify flood events for the purposes of parametric insurance products. Such products, also known as weather-index insurance for this specific case, aim to compensate for the related losses right after a flood event. Point (2) above is not necessarily present within near real-time loss estimation models, and, in such circumstances, a pre-determined payout is paid by the insurance regardless of the actual loss.

It is worth noting that the methodology presented in this study could also be adapted for early warning purposes (e.g., different alert levels could be pre-defined based on the modeled event size). However, it is specifically designed in this study to serve as a basis for parametric insurance products.

This paper represents an extension of a previous study of the authors (Vecere, Martina, Monteiro, & Galasso, 2019), where the proposed methodology was broadly presented. However, the present paper includes additional sensitivity analyses on the model parameter optimal configuration and a location accuracy analysis, given its relevance in the context of parametric insurance, for which the proposed SPEED model is designed.

1.1 Satellite Precipitation-based Extreme Event Detection (SPEED)

The trigger employed in the proposed SPEED model should satisfy the following criteria: (1) accessibility in near real-time; (2) adequate temporal coverage to compute meaningful statistics on it (i.e., typically 20 years); (3) accuracy and consistency over time of the methodology underlying the estimation of the environmental variable (i.e., precipitation); (4) marked correlation between the selected trigger and the associated losses (Figueiredo, Martina, Stephenson, & Youngman, 2018). Additional advantages of using satellite data are their global coverage (i.e., no need for local recording stations), the free data accessibility, and the use of a tamper-proof trigger. The latter aspect, in particular, represents an added value with respect to traditional parametric coverages whose payout is based on data retrieved from measurement networks/recording stations (i.e., rain gauges) around a target site. Furthermore, a considerable premium reduction could be obtained by spreading the risk over large regions.

Based on these preliminary remarks, this paper proposes a methodology to identify loss-triggering events through satellite precipitation data. Event detection is a crucial aspect in any near real-time loss estimation model to ensure accuracy and precision. One of the advantages of using a model to identify a loss event is the statistical consistency of the loss occurrence

both in the pricing phase (i.e., premium computation) and during the model operation (i.e., payout settlement). Indeed, under the assumption of stationarity conditions, if the data source used in the calibration/validation phase (historical observation) is the same as the one employed for the operational phase of the model (i.e., homogeneous dataset), the probability distribution of the loss computed for the pricing phase is consistent with the frequency of occurrence of the actual loss, upon which the payout settlement depends. This feature is particularly convenient when the model is used within a parametric insurance program because the estimated annual average payout of the operational period is the same as the historical period. Therefore, the price for the insurance (premium) is consistent with the payouts. Conversely, traditional insurance uses catastrophe models to estimate the annual average payout (and price the contract), but uses other procedures (e.g., loss adjustment) to compensate for the actual loss. Hence, the proposed SPEED model differs from traditional risk assessment models and, particularly, from different available post-disaster impact methodologies, such as the Prompt Assessment of Global Earthquakes for Response (PAGER) or the Global Disaster and Alert Coordination System (GDACS) web-based disaster information systems (Mehta, 2017; Wald, Jaiswal, Marano, Bausch, & Hearne, 2010).

Specifically, the proposed SPEED model belongs to the category of the so-called early or rapid loss estimation models, which aim at providing an estimate of the impact/loss in a given area, following a natural-hazard event (such as floods or storms), within a few hours or days. These models can be classified into two main categories depending on the data used to assess the loss of the event:

i) Models using observations of effects or impacts of the event on the territory;
ii) Models employing environmental variables related to the hazard intensity.

The first category includes, for instance, flood-mapping methodologies that leverage optical imagery, such as the Moderate Resolution Imaging Spectroradiometer (MODIS) products from Terra and Acqua satellites (G R Brakenridge, Andersona, Nghiemb, Caquard, & Shabaneh, 2003; R. Brakenridge & Anderson, 2006), or radar sensors such as Sentinel, which offer the advantage to penetrate clouds, differently from the former. Two notable examples of flood mapping through MODIS data are represented by the near real-time Global Flood Mapping Project (GFMP) (Slayback, Brakenridge, & Policelli, 2012) and the Dartmouth Flood Observatory (DFO) (G. Robert Brakenridge, 1993). Optical imagery is also used to compute vegetation indices like the Normalized Difference Water Index (NDWI), as in the 'Using Satellites to Make Index Insurance Scalable' project mentioned above, among others. Land-surface and hydrologic models are also employed to estimate flood impact, as in the Global Flood Monitoring System (GFMS) (Wu et al., 2014). Finally, in recent years, several studies investigated the potential behind social media - which falls in the category of the so-called volunteered geographic information - for DRM purposes and particularly in the emergency response phase (Poser & Dransch, 2010), for instance in (Fohringer, Dransch, Kreibich, & Schröter, 2015).

The second category of early or rapid loss estimation models includes those leveraging environmental variables related to the hazard intensity by defining specific thresholds to then identify extreme events (and, possibly, provide an estimate of their impact). For example, peak discharge or rainfall are generally (and widely) used as a trigger for flood events.

One model using rainfall as a trigger is the one provided by the Excess Rainfall (XSR) risk model, developed for CCRIF (introduced above) over the Caribbean region (CCRIF SPC, 2018). CCRIF launched the first excess rainfall parametric insurance product in 2013, later updated in 2016, when a new model was released, namely CCRIF Excess Rainfall Model 2.0. This model simulates the amount of precipitation over the Caribbean area in near real-time based on a combination of climatic-meteorological models and a low-orbiter satellite-based precipitation model to produce a rapid estimate of the potential losses (CCRIF SPC, 2016). If the rainfall policy is triggered for one of the countries that have purchased XSR coverage, a payout based on the CCRIF insurance policy conditions is issued to the affected nation. The key novelty introduced by this model is the estimation of rainfall-induced losses to the modeled exposure rather than only using event parameters (as in traditional parametric insurance contracts). Excess of rainfall coverage - in addition to drought - is also provided by the Pacific Rapid-Response Financing program initiated by the World Bank on behalf of Pacific Island Countries (PICs). Drought and rainfall indices were developed using satellite data from the National Aeronautics and Space Administration (NASA). To this end, a prototype web-based monitoring system was designed to automate rainfall data processing in near-real-time (GFDRR, 2018). Another interesting example of rapid loss estimation models is the one adopted by the meso-level index-based flood insurance for the Sirajganj district in Bangladesh (Oxfam, 2013). The product uses model-generated flood data for payout calculation. In this way, the product is scalable and free from tampering and human errors, as in the case of a water level gauge network. The Institute of Water Modeling (IWM) based in Bangladesh developed a dedicated 1-D hydrodynamic model to generate both historical water levels in the river channels and flood plains as well as post-event data used for payout computation. Once discharge and water levels in correspondence of rivers and channels have been computed, the model uses a 1D-2D coupled model (MIKE flood model) and a digital elevation model (DEM) to produce flood maps and water level data over the flood plain. The compensation payment schedule is based on the number of continuous days of flood at a single household level.

The SPEED model proposed in this study belongs to the second category of rapid loss estimation models. They are intended to overcome the limitations posed by models of both typologies described above, namely:

- dependence upon atmospheric conditions, such as clouds in the case of optical imagery;
- long revisit time and limited area coverage provided by radar sensors;
- use of complex hydraulic or hydrological models that are computationally expensive and time-consuming;
- combination of forecast and satellite-based precipitation models.

SPEED models are specifically designed to fill such gaps in existing rapid loss estimation modeling through the following features:

- the use of satellite precipitation estimates only to streamline the process of event identification, thus providing timely inputs for parametric coverages;
- a reliable and intuitive framework composed of sequential steps – as discussed later – where a combination of different thresholds based on satellite precipitation estimates is employed;
- global coverage and high spatial and temporal resolution due to the intrinsic characteristics of the selected trigger;

- high flexibility with possible integration of new satellite precipitation datasets or inclusion of additional environmental variables/satellite products.

In the remainder of this paper, the proposed SPEED-based framework is applied to identify flood events over the Philippines. After describing the selected reference database for historical hydrometeorological events in the country, the designated trigger is investigated with particular reference to its suitability to the SPEED-based methodology introduced in the paper. Then, model construction (i.e., the definition of its methodological steps) and calibration are thoroughly presented. Model performance is finally evaluated, and its optimal configuration is defined based on those model parameters (i.e., thresholds) that minimize basis risk over the designated study area. To further demonstrate the proposed methodology's added value, event localization accuracy within specific macro-areas is also investigated.

2 Methodology

The methodology developed to detect hydrometeorological events here applied to the Philippines and conceptually depicted in Figure 1 is detailed in the following. Firstly, the model event definition procedure and the computation of the optimal thresholds for identifying flood events according to the proposed methodology are described. Then, the model skills are investigated in terms of both extreme events detection and the accuracy of their location with respect to historical information.

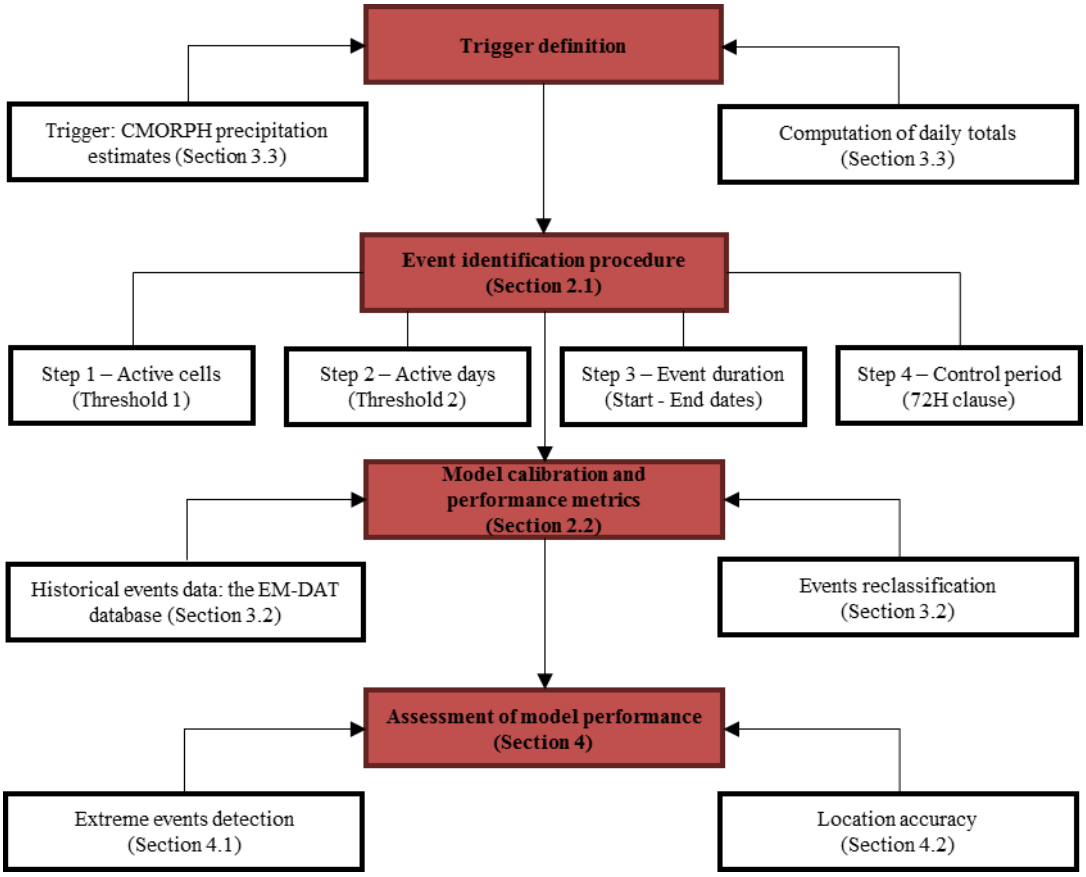

Figure 1: Conceptual framework of the proposed model. The main phases of model development are highlighted in red.

2.1 Event identification procedure

The methodology developed to identify extreme meteorological events over the Philippines' territory, which employs daily precipitation as a primary trigger, consists of four sequential phases:

1. Identification of active cells over the investigated region;
2. Computation of active days within the selected timeframe;
3. Definition of event duration (i.e., start and end event days);

4. Event detection within a pre-defined control period.

A single cell is considered active when its daily precipitation value exceeds a specific threshold, which is hereafter referred to as Threshold 1 (Thr.1), as illustrated in Figure 2.

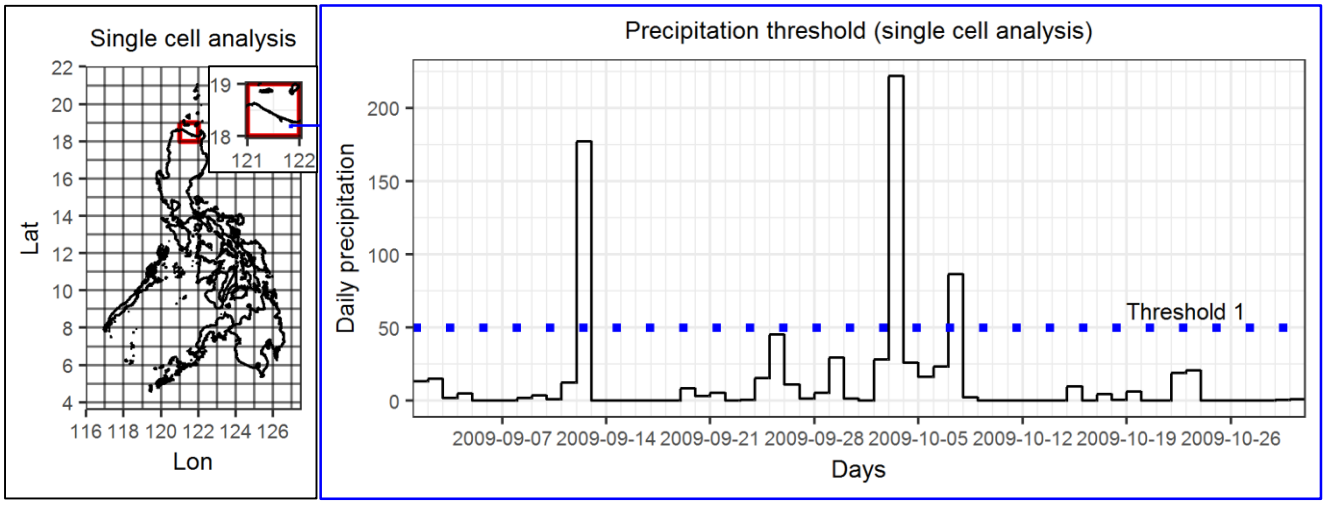

Figure 2: Identification of active cells.

In the second step, another threshold, Threshold 2 (Thr.2), is defined on the total number of active cells (or cell percentage) within each day, and it is used to determine if an event occurred in a given day (Figure 3). Both thresholds are selected from a range of possible values through the procedure presented in the following section.

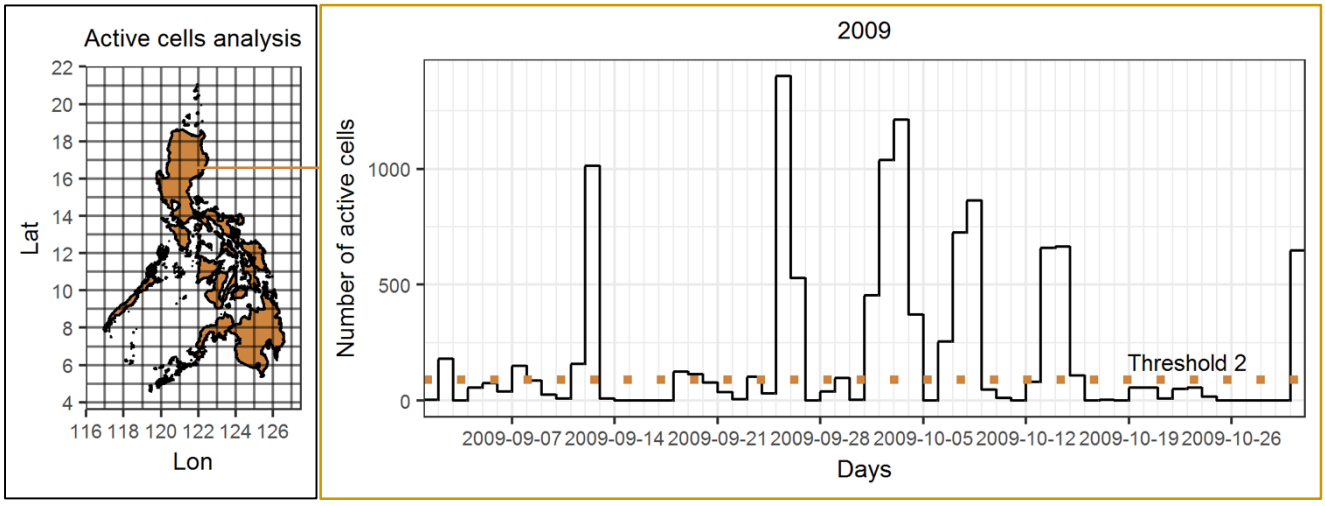

Figure 3: Identification of active days.

The third step aims to define event duration due to the active days specified in the previous phases. The event starts on the first active day and ends on the day in which the active cells count is lower than Threshold 2 (Th.2) with the inclusion of tolerance (a single day in this case). Figure 4 illustrates the event start and end dates definition.

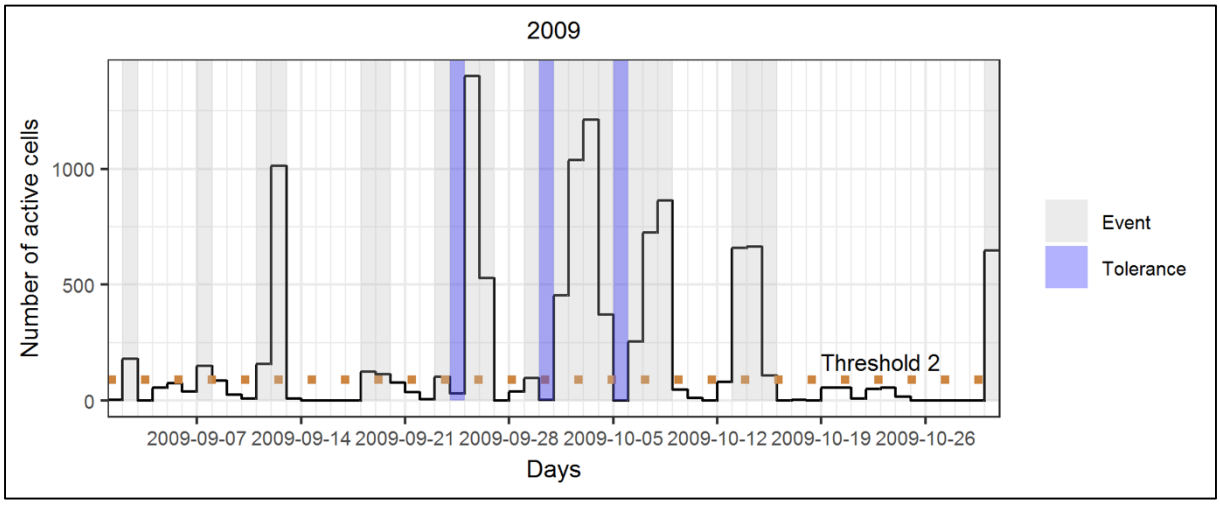

Figure 4: Event definition with the highlighted period of tolerance.

The fourth and last step of the procedure corresponds to the definition of a control period to assess if an event has occurred. Two main reasons justify the adoption of a period longer than one day to check estimated events with respect to the historical (real) ones. Firstly, considering the islands' size, the duration of a flood event is approximately three days. Secondly, in the insurance policy, the so-called "72-hour clause" (Chartered Insurance Institute, 2017; Clarke, 2018) considers all the losses that occurred within 72 hours from the first event as a single claim. Any event duration exceeding three days is represented as a multiple of this aggregation period.

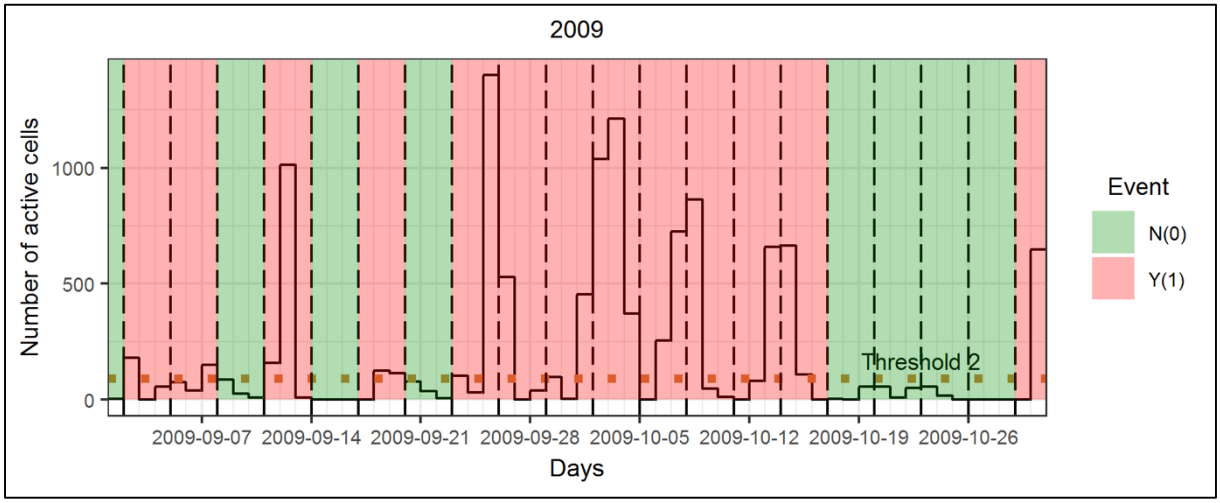

Figure 5: Event definition with the highlighted period of tolerance.

This type of constraint is often imposed on weather-related perils, such as storms or floods, and to other catastrophes, such as earthquakes, to conventionally define a claim's time duration. Therefore, a three-day aggregation was adopted in this study (Figure 5). Subsequently, an event's occurrence is established based on the presence of at least one active day within the control period, which is then translated into a binary array of simulated events.

2.2 Model calibration and performance metrics

The model is calibrated to determine the optimal combination of Thr.1 and Thr.2 values introduced above. Two sets of values were defined to include the broadest range of reasonable entries for both thresholds. In particular, Thr. 1 varies between 1 and 100mm with 5mm interval, whereas Thr. 2 can assume values from 1% to 15% with 0.5% interval. The combinations of the two sets of values for both thresholds produced a total of approximately 640 runs. A bootstrapping method, which will be thoroughly described in Section 4.1, is used to identify the best model configuration among all the above-mentioned runs.

Table 1: Contingency table.

		Real events
Modeled events	*Yes*	*No*
Yes	*Hits*	*False Alarms*
No	*Misses*	*Correct Negatives*

The combination of the two thresholds aims to create the binary vector of simulated events described above, which needs to be checked against the same binary array produced for the real events with the same assumption of a three-day control period for consistency with model simulation. These two arrays are the basis for generating the so-called contingency table (Table 1), following a procedure traditionally used in the weather forecast verification field (Stanski, Wilson, & Burrows, 1989). The 'hits' is defined as the number of events captured by the model which actually took place. 'Misses' represents the number of real events the model was not able to identify. The 'False alarms' refers to the number of events wrongly detected by the model since they did not actually occur. 'Correct negatives' entry is the number of events that were correctly identified by the model as non-events. Model performance skills were assessed by using two metrics, namely the Probability of detection (POD) and the Probability of false detection (POFD), which are defined, respectively, by Eq. (1) and (2):

$$POD = \frac{Hits}{Hits+Misses} \tag{1}$$

$$POFD = \frac{False\ alarms}{False\ alarms+Correct\ Negatives} \tag{2}$$

The POD computes the portion of the observed "yes" events correctly captured by the model, whereas the POFD returns the fraction of the observed "no" events the model wrongly classifies as "yes" events.

A Skill Score (SS) coefficient can also be defined to provide a synthetic metric to evaluate the model. It is defined as the difference between the statistical quantities previously defined, according to Eq. (3).

$$SS = POD\text{-}POFD \tag{3}$$

Therefore, from a probabilistic point of view, the skill score represents the difference between the probability of detection and the probability of false detection. Ultimately, it is a measure of the model's accuracy, providing an estimate of the model's ability to discriminate between events and non-events.

3 Case-study area and input data

3.1 The Philippines' risk profile

The Philippines is an archipelago of more than 7000 islands covering an area of approximately 300,000 Km^2. The country is one of the most disaster-prone countries worldwide, being exposed to different types of natural hazards (Figure 6a). The 2020 *Germanwatch Climate Risk Index* confirmed this by ranking the Philippines 2nd worldwide among the most affected countries by events in 2018 and 4th in the period 1999-2018 (Eckstein, Künzel, Schäfer, & Winges, 2019). Due to its geographical location, it is exposed to various geological hazards (earthquakes, landslides, volcanic Eruptions, etc.), especially to hydrometeorological risk, namely floods, typhoons, and seasonal rains. For this reason, the national government has primarily

invested in developing *ex-ante* financial mechanisms aimed at mitigating the impact of those events and increasing the country's resilience to natural hazards (e.g. (D'Ayala et al., 2020; Sevieri et al., 2020)).

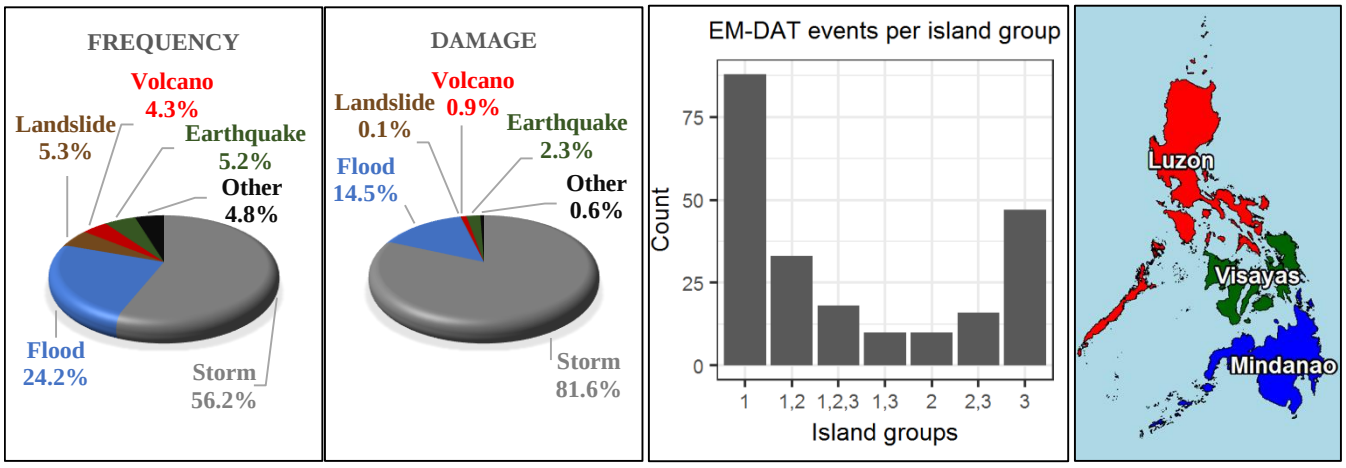

(a) **(b)** **(c)**

Figure 6: Hydrometeorological events in The Philippines according to EM-DAT in terms of (a) frequency, (b) damage, and (c) event location by island group (Luzon = 1, Visayas = 2, Mindanao = 3) between 1998 and July 2017.

3.2 Historical events data: the EM-DAT database

Historical events information was obtained from the Emergency Events Database (EM-DAT) (D. Guha-Sapir, 2020), a data collection for over 22000 disasters globally from 1900 to the present. In addition to the date and location of each event, the database defines the event typology (e.g., flood - fluvial flood, storm - tropical cyclone - convective storm), and, where this detail is available, it provides additional disaster information such as the event footprint area, hazard magnitude (e.g., maximum wind speed) or location coordinates (e.g., earthquake epicenter's latitude and longitude). EM-DAT collects several types of information to measure event impacts such as the number of dead people (i.e., total deaths), total affected people (defined as the sum of affected, injured, and homeless people), and total damage, which includes direct and indirect economic losses as well as damage to property, crops, and livestock (Figure 6a).

For the present study, a reference dataset for model calibration and validation was created by collecting historical hydrometeorological events in the Philippines. The original 493 events were filtered to select only events from January 1998 to July 2017, to match the period covered by the reference precipitation dataset used in this study. This resulted in a final database of 222 events. Those events were finally reclassified according to the island group where they occurred. Following the country's coarsest administrative subdivision, indeed, three different regions were defined: Luzon, Visayas, Mindanao. (Figure 6b/c).

3.3 Trigger: CMORPH precipitation estimates

The trigger used within the proposed SPEED model is represented by the CMORPH (CPC MORPHing technique) daily precipitation estimates. CMORPH precipitation estimates are provided from 1998 onwards and cover the area between 60°S – 60°N latitude. It combines 30 minutes temporal with 8 km spatial resolution. CMORPH precipitation estimates are also available with a short latency of just 18 hours after acquisition.

This precipitation dataset is named after the so-called "morphing" technique used to produce precipitation estimates by relying exclusively on low-orbiter satellite microwave observations whose spatial propagation information is derived from geostationary satellite InfraRed (IR) data (Joyce, Janowiak, Arkin, & Xie, 2004). This dataset was selected because of its combination of high spatial resolution and low latency (i.e., data availability after the acquisition). Indeed, even if other precipitation datasets featuring longer temporal coverage are available, such as the Climate Hazards Group InfraRed Precipitation with Station data - CHIRPS (Funk et al., 2015), NASA's MERRA-2 (Gelaro et al., 2017) or ECMWF's ERA5(T) (Hersbach et al., 2020) covering a period from 1981, 1980 and 1979 to present respectively, they have a longer latency ranging from five days to two-three weeks after the month of acquisition, making these products inappropriate for near-real-time applications.

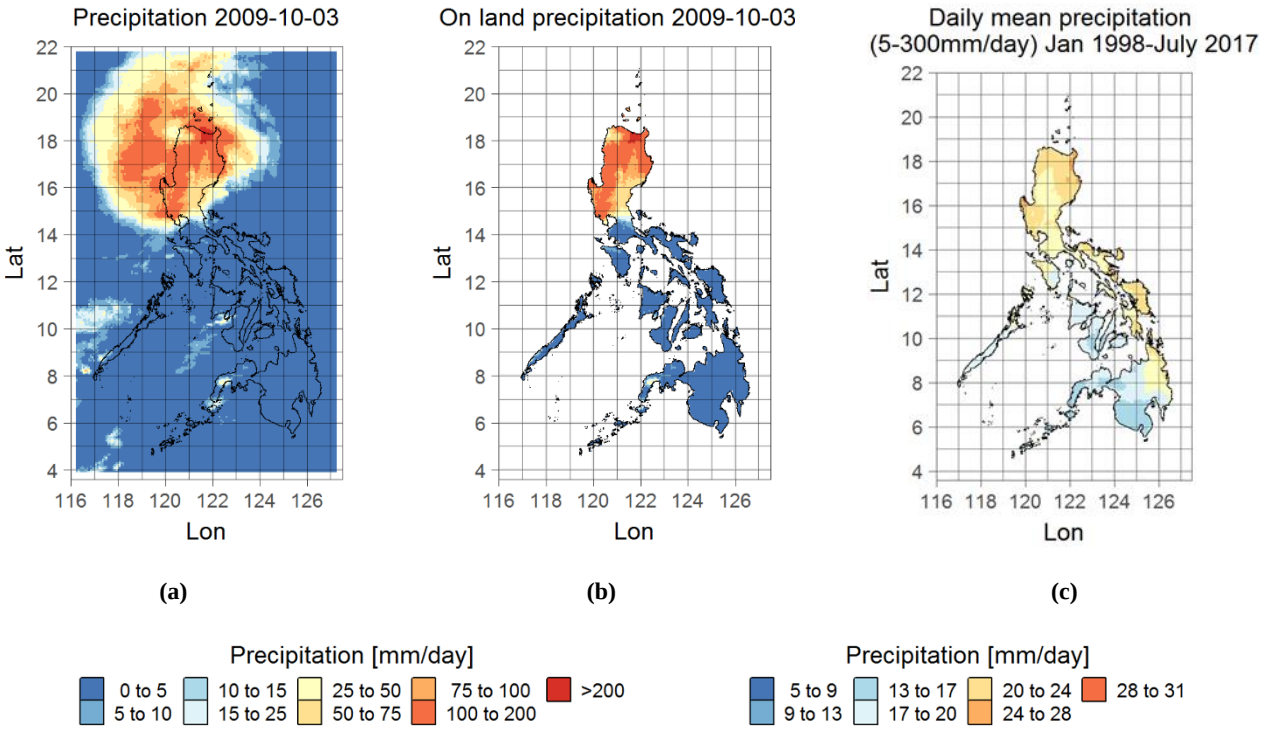

Figure 7: CMORPH precipitation on 2009-10-03 over the Philippines (a) and on the country's land only (b). Daily mean precipitation values between 1998-01 and 2017-07 (c).

A specific code was developed in the R programming language (R version 3.5.1 and RStudio 1.1.453) to process the original half-hourly data and produce the final daily precipitation values. CMORPH data was firstly cropped over a rectangular area around the country (Figure 7a), where daily precipitation values were computed. Consequently, a filter was applied to extract precipitation estimates on land (Figure 7b). As a result, a grid featuring 4630 cells for each day within the covered period was produced. A map featuring the mean daily rainfall within the investigated period is also included to highlight areas most impacted by intense precipitation (Figure 7c).

4 Assessment of model performance

4.1 Extreme events detection

Model calibration (training) and testing is performed using a bootstrapping method applied over the whole investigated period (January 1998 – July 2017). In particular, model training is performed by selecting recursively 18 years and testing the model on the additional two years. Table 2 summarizes the different training and testing periods that were investigated.

Table 2: Training and testing periods.

Bootstrapping run	Training period	Test period
1	2000-2017	1998-1999
2	1998-1999, 2002-2017	2000-2001
3	1998-2001, 2004-2017	2002-2003
4	1998-2003, 2006-2017	2004-2005
5	1998-2005, 2008-2017	2006-2007
6	1998-2007, 2010-2017	2008-2009
7	1998-2009, 2011-2017	2010-2011
8	1998-2011, 2014-2017	2012-2013
9	1998-2013, 2016-2017	2014-2015
10	1998-2015	2016-2017

For each training period, all the different model configurations resulting from the various combinations of Thr.1 (from 1 to 100mm with 5mm increments) and Thr.2 possible entries (from 1% to 15% with 0.5% steps) were run. Then the results are ranked based on the skill score (SS), and the configurations with the highest SS value are derived (Table 3). Based on the results reported in Table 3, the best model configuration for almost all investigated training periods (except the period 1998-2015, for which it is the second-best model configuration) is Thr. 1 = 65mm/day and Thr. 2 = 2%.

315

Table 3: Best model configurations on training periods (bootstrapping).

Bootstrapping run	Thr. 1 [mm/day]	Thr. 2 [%]	SS	Training periods
1	65	0.02	0.603	2000-2017
2	65	0.02	0.611	1998-1999, 2002-2017
3	65	0.02	0.598	1998-2001, 2004-2017
4	65	0.02	0.581	1998-2003, 2006-2017
5	65	0.02	0.584	1998-2005, 2008-2017
6	65	0.02	0.619	1998-2007, 2010-2017
7	65	0.02	0.625	1998-2009, 2011-2017
8	65	0.02	0.610	1998-2011, 2014-2017
9	65	0.02	0.593	1998-2013, 2016-2017
10	40	0.05	0.606	1998-2015

Therefore, these threshold values (Thr. 1 = 65mm/day, Thr. 2 = 2%) were then used to assess the model performance over all the testing periods. Table 4 contains the results of these analyses: the highest skill score was obtained for the years 2004-2005,
320 whereas the lowest skill score resulted from testing over the period 2008-2009. These results are possibly due, among other factors, to the different number of reported real events in those periods: 15 events in 2004-2005 and 41 events in 2008-2009.

Table 4: SS results over all test periods with Thr. 1 = 65mm/day and Thr. 2 = 2% (bootstrapping).

Bootstrapping run	POD	POFD	SS	Test periods
1	0.900	0.254	0.645	1998-1999
2	0.815	0.278	0.537	2000-2001
3	0.840	0.187	0.652	2002-2003
4	0.999	0.136	0.863	2004-2005
5	0.892	0.126	0.766	2006-2007
6	0.741	0.243	0.498	2008-2009
7	0.703	0.200	0.503	2010-2011
8	0.762	0.214	0.548	2012-2013
9	0.857	0.167	0.689	2014-2015
10	0.619	0.304	0.551	2016-2017

325 Finally, model skills are assessed over the entire analysis period (1998-2017) by considering all combinations of Thr. 1 and Thr. 2. The top ten model configurations, i.e., the ones producing the highest SS values, are reported in Table 5.

Table 5: Top 10 model configurations over the entire investigated period (no bootstrapping).

	POD	POFD	Thr. 1 [mm/day]	Thr. 2 [%]	SS
1	0.804	0.201	65	0.02	0.603
2	0.797	0.197	60	0.03	0.600
3	0.798	0.209	55	0.03	0.589
4	0.838	0.250	40	0.05	0.588
5	0.737	0.151	50	0.05	0.586
6	0.732	0.148	45	0.06	0.584
7	0.761	0.178	45	0.05	0.583
8	0.735	0.152	60	0.03	0.583
9	0.836	0.253	55	0.03	0.582
10	0.821	0.240	35	0.07	0.581

This analysis confirms the best model configuration obtained for the threshold values presented above (Thr. 1 = 65mm/day and Thr. 2 = 2%). Higher skill scores are obtained in correspondence of high daily precipitation values (Thr. 1 between 55 and 65 mm/day for the three best configurations) and a low number of active cells (Thr. 2 between 2% and 3% in the same cases). The SS values higher than 0.6 reported above for the best model configurations are deemed satisfactory since they indicate that the model is capable of correctly detecting more than 80% of observed real events (i.e., POD), while it wrongly classifies as flood events only about 20% of the observed non-events (i.e., POFD). However, it has to be noticed that the whole model performance - that is, the results associated with all tested combinations - must be analyzed to fully assess model skills in flood event identification. This will be discussed later through specific forecast verification measures (i.e., ROC curve).

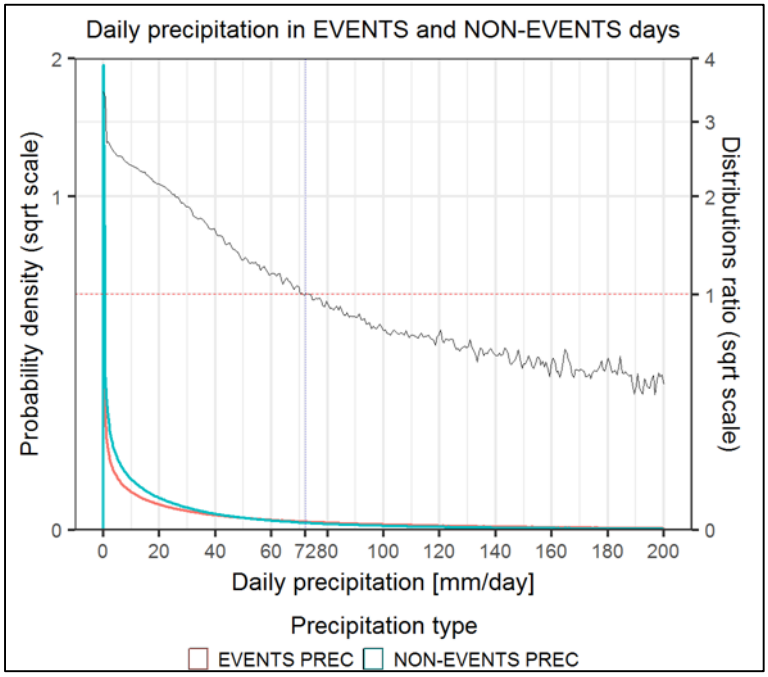

Figure 8: Conditional distribution of CMORPH precipitation in event and non-event days (the continuous black line represents the distribution ratio; the red dashed line indicates where the ratio is equal to 1).

Kernel frequency density estimates are used to represent the daily cumulated precipitation occurred in non-event days (i.e., non-events precipitation) and the one that caused a flood (i.e., events precipitation) with the addition of a polyline depicting the ratio between non-event and event precipitation density values (see Figure 8). The ratio between the two distributions indicates that the floods are typically associated with high precipitation and specifically to daily values above 72 mm/day, where the above-mentioned measure is lower than 1. This proves that, as expected, there is a strong correlation between flood events and elevated daily precipitation values.

The accuracy of the binary outcome predictions was also assessed through the relative operating characteristic (ROC) curve. It provides a graphical representation of POD and POFD when considering different values for Thr.1 and Thr.2. Specifically, the model performance can be assessed considering the area underneath the ROC curve - Area Under Curve (AUC). A perfect model exhibits a ROC curve that goes from the bottom left (0,0) to the top left (0,1) of the diagram and then across to the top right (1,1). In this case, AUC is equal to 1. AUC can assume values between 0 and 1, with 0.5 indicating a random model, for which the ROC curve is a diagonal line from bottom left (0,0) to top right (1,1). The proposed SPEED model exhibits a very good predictive capability, given that the ROC curve is remarkably far from the diagonal line (that refers to a perfectly random model). This is also reflected in the high value for the AUC parameter (0.86), thus confirming the very good model performance. In this case, the ROC curve is presented as a cloud of points (Figure 9), with each of them representing a different model configuration. The highest variability is found around the optimum model configuration, which typically is defined as

the model configuration associated with the point featuring the highest distance from the diagonal line. Indeed, this point represents the model with the best performance with respect to a completely random model (diagonal line). It is also worth noting that model configurations with the highest Thr. 1 and Thr. 2 are located in the bottom-left part of the plot, where both POD and POFD are lower. Conversely, model configurations obtained for lower precipitation (Thr. 1) and active cells threshold (Thr. 2) values lie in the top right corner, given that, as expected, for such a configuration, the number of hits and false alarms is maximized.

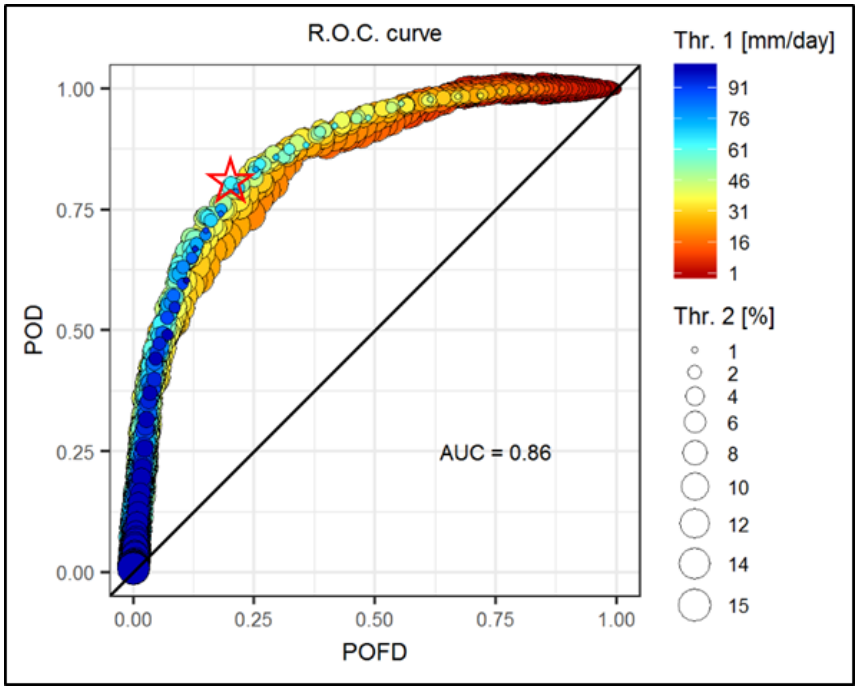

Figure 9: ROC curve and AUC (each point represents a different model configuration).

4.2 Location accuracy

The model's capability to correctly identify where a specific event has occurred is also tested, in addition to the model performance in accurately detecting the occurrence of a flood event. This aspect is crucial to correctly determine where a flood event has actually taken place and timely direct resources to the affected area. Indeed, in some cases, the payout associated with parametric insurance programs is managed by a central national authority, which oversees the assigned budget for emergency operations to the smaller administrative units that suffered the most extreme event consequences. The accurate identification of the affected area (or macro-area, here defined as island groups) can thus be important, firstly, to address the funds directly to the affected zones (where this is consistent with the country's emergency management legislation) and, secondly, to speed up the actual availability of resources for the interested administrations.

As such, a procedure aimed at determining the island group, as defined earlier, hit by each detected event, is developed and presented here. The starting point for the event localization is the daily precipitation, similar to what is described above for its

identification. For each day of a modeled event, the portion of rainfall above the precipitation threshold of the optimal configuration (65mm/day) is extracted, which previously have been defined as active cells, as illustrated in Figure 10.

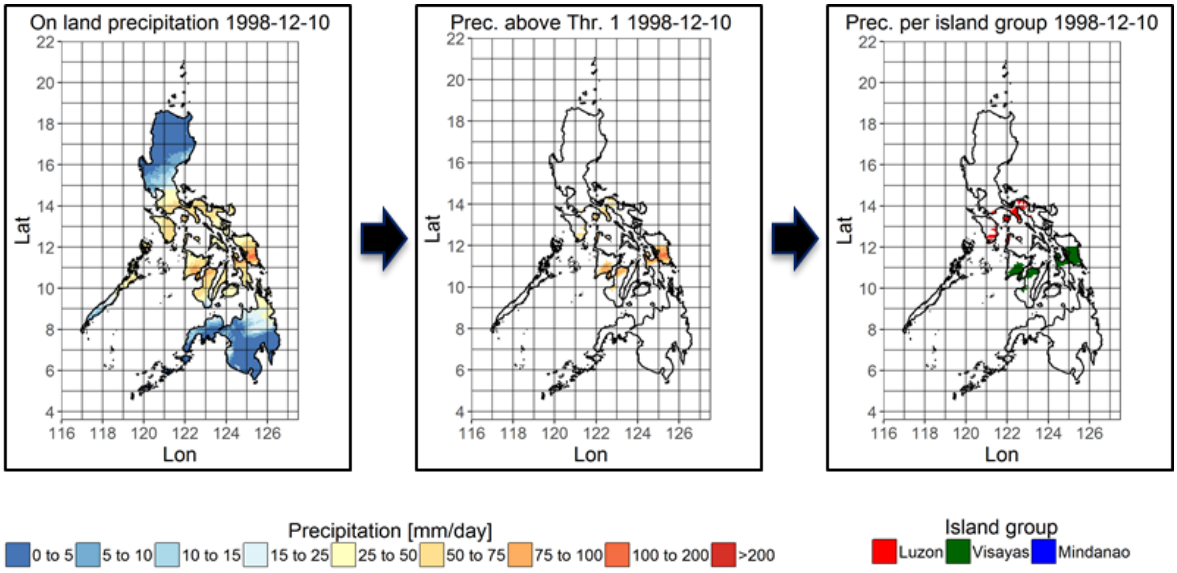

Figure 10: Event localization procedure for a generic event day.

Given that an event typically lasts more than a single day, the sum of the active cells over all the event days is computed to produce the total number of active cells per event. Then, the share of the active cells per event over each of the three above-defined island groups (Luzon, Visayas, and Mindanao) is computed. The criterion adopted here to assign an event to a specific island group is that at least 30% of the event active cells are located on a single island group (Figure 10). This percentage was chosen based on the country's selected number of macro-areas (i.e., three, hence $1/3 \approx 30\%$) where the localization check was conducted.

As mentioned earlier, the original EM-DAT hydrometeorological events for the investigated period have been manually reclassified to conduct a verification of the model accuracy on event localization. The optimal model configuration, featuring Thr. 1 = 65mm/day and Thr. 2 = 2%, correctly detected 169 events out of the initial 222.

Table 6: Localization results for modeled and real events (L = Luzon, V = Visayas, M= Mindanao).

	Modeled events								
Real events	**L**	**V**	**M**	**L,V**	**L,M**	**V,M**	**L,V,M**	**Tot.**	**Acc. [%]**
L	54	1	0	5	2	0	0	**62**	**87%**
V	1	3	1	1	0	1	0	**7**	**43%**
M	7	1	9	4	1	6	0	**28**	**32%**
L,V,	16	1	0	12	1	0	1	**31**	**39%**
L,M	7	1	1	0	1	0	0	**10**	**10%**
V,M	1	3	1	3	1	5	0	**14**	**36%**
L,V,M	2	2	2	4	2	5	0	**17**	**0%**
Tot.	**88**	**12**	**14**	**29**	**8**	**17**	**1**		

The comparison between the location of modeled events (in the optimal configuration) and the corresponding real (historical) events is reported in Table 6. For each of the two types of events, the single island groups, as well as their combinations, are considered. The highlighted diagonal reports the direct matching results between model and observations. Column and row totals have also been included, with an additional column reporting the percentage of real events correctly detected by the model for each island group or their combinations (i.e., localization accuracy). Figure 11 depicts a Venn diagram representation of localization results for modeled and real events, including the share of modeled/real events for all individual and combined island groups.

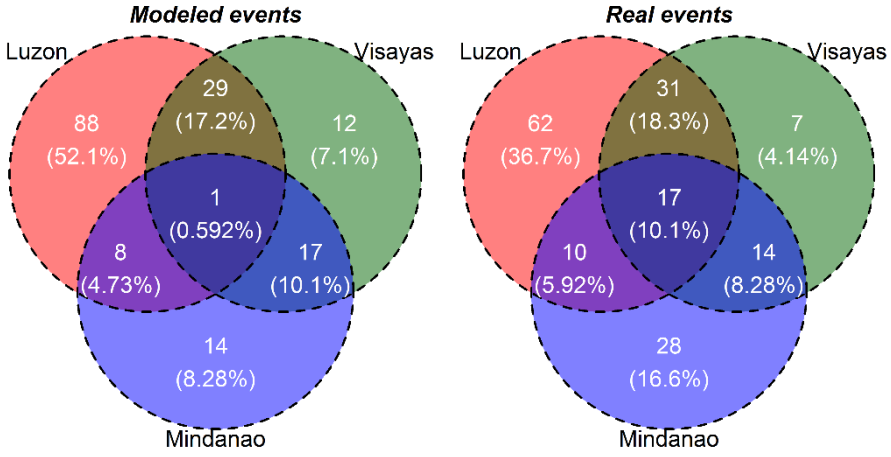

Figure 11: Venn diagram representation of localization results for modeled and real events.

The island group that reports more events is Luzon, with a total of 62 real events. The model correctly detected 54 of them, corresponding to a remarkable accuracy of 87% in this area. The first row of Table 6 also reports five events that the model attributed to Luzon and Visayas groups and two events on both Luzon and Mindanao groups. The number of events that the model located in the Luzon group is also in agreement with both the high number of registered events there and the map of daily average precipitation presented before (Figure 7c).

The total number of detected real events of the Visayas group is lower than the one for the previous group with just seven real and 12 modeled events. In this case, the accuracy is lower, with only 43% of correctly detected events over the Visayas group. This percentage decreases further to 32% in the Mindanao group (corresponding to nine events). This is a consequence of the lower absolute number of events (particularly for Visayas events) in these island groups, which makes the associated accuracy measurement less statistically significant. Furthermore, because of their low absolute number, events that occurred on Visayas and Mindanao are also affected by greater uncertainties in terms of the association to specific island groups. In this sense, for example, it must be noted that the model assigned seven events to pairs of island groups including Mindanao (i.e., L,M and V,M), which according to EM-DAT took place on that specific island group. If those events were added to the nine correctly detected on the Mindanao island group, this would substantially increase the overall model accuracy in that area.

When analyzing the results of the events that occurred on multiple island groups, the best performance is obtained for the Luzon-Visayas with 12 events correctly identified (39% of total real detected events in that area), but with additional 16 events on the Luzon island group, which can be seen as an additional partially corrected events location. In the Luzon-Mindanao group, the total number of real events that occurred there and correctly captured by the model decreases. The same decreasing trend is observed in the share of events the model assigned to this group combination, but, again, with many events located on the Luzon group (seven out of 10 total real events). The model performance improves for the Visayas-Mindanao group combination with 36% accuracy (five events over a total of 14 historical ones occurred here, with additional four events located by the model in at least one of the Visayas or Mindanao groups).

The last group combination considers events affecting all the three investigated island groups. This is a very particular situation, which the model seemed to be less capable of capturing since no historical events affecting the whole country were correctly detected. Moreover, the model identified only one event on all three island groups, which, according to EM-DAT, affected only the Luzon and Visayas group. The high uncertainty on the identification of events on multiple island groups and particularly on events covering the whole country (all island groups) underlines the need for further investigation on the EM-DAT events location definition and the analysis of additional sources of information on the area affected when multiple island groups are considered. For instance, the proposed model does not consider the effect of wind, which could affect areas different from those subjected to extreme precipitation. This circumstance cannot be captured by the proposed model, which relies exclusively on precipitation measures.

5 Conclusions

This study introduced a Satellite Precipitation-based Extreme Event Detection (SPEED) model for managing flood risk, here applied to the Philippines as a case study country. This type of model can be readily employed in parametric insurance programs or weather-index insurance, whose ultimate goal is to quickly provide financial liquidity to affected countries for immediate emergency assistance such as shelters, food, and medical supplies.

Models, such as the proposed SPEED one, usually rely on one or more triggers to identify an event. For the considered case study, the selected trigger for SPEED consist of CMORPH satellite precipitation estimates, which met the requirements that are typically set for this type of models: availability in near real-time (18 hours latency), long temporal coverage (20 years from 1998 to July 2017), low temporal (30 minutes) and spatial (approximately 8 km) resolution. Considering the availability of a large number of hydrometeorological events for the Philippines, the EM-DAT database was used as a source of reported loss events for model calibration and validation. The proposed methodology, specifically intended to identify flood events, started from the definition of active cells - by setting a precipitation threshold (Thr. 1) on daily computed precipitation for each grid cell - which were then used as a basis for the identification of the so-called active days. To this end, a second threshold on the number of active cells - Thr. 2 - was used. The event start and end dates were then defined, with the inclusion of a tolerance period. Finally, a control period of three days was defined to determine whether or not an event had occurred for consistency with standard insurance coverage practice related to this kind of extreme events.

The proposed model's performance was assessed using forecast precipitation verification methodologies available in the literature, such as the Probability of detection (POD), the Probability of false detection (POFD), and the Receiver operating characteristic (ROC) curve. Furthermore, the model was calibrated and validated using a bootstrapping method over 20 years of precipitation data. Training and testing were performed recursively over 18- and 2-year intervals, respectively. A total of 10 best pairs of values for both thresholds (model configurations) were selected and evaluated. In almost all the investigated periods (except for the test period 2016-2017, most probably also because the period of testing was lower than the other periods, as it was limited to July 2017), the model configuration best performing was the one featuring Thr. 1 = 65mm/day (threshold on precipitation of a single cell) and Thr. 2 = 2% (limit posed on the number of active cells over the whole country). A skill score was also quantified as the difference between POD and POFD to measure the model capability to detect flood events in the Philippines, featuring a remarkable average value above 0.6 among all investigated test periods. The precipitation conditional distribution analysis in event and non-event days showed that it could be employed as a reliable predictor for flood events. The ROC curve, which resulted from a total of approximately 640 different model combinations (of Thr. 1 and Thr. 2) over the entire investigated timeframe, indicated an adequate capacity of the model to detect flood events in the Philippines with an area under curve (AUC) equal to 0.86. It also confirmed the results of the calibration phase in terms of optimal threshold combinations.

Moreover, the model was also assessed in terms of localization accuracy. In this sense, the results indicate an excellent model performance in detecting events on single island groups, especially on the Luzon island group, the one that is most subjected

to extreme hydrometeorological events, as denoted by the observation of the mean daily precipitation maps. Lower accuracy in detecting events assigned to the Visayas and Mindanao island groups was observed instead. Conversely, the identification of events on two or three island groups proved to be more challenging, specifically when all three island groups were interested as well as in the case of events affecting the northern and southern island groups, that is, respectively, Luzon and Mindanao. Considering the above, the detection of events occurring on several island groups would certainly require additional research. Further investigation of the areas historically affected by flood events is needed to countercheck the EM-DAT event location, when multiple island groups are of interest, to understand better the typically higher uncertainty affecting situations of this sort. This is particularly evident in the case of events that, according to EM-DAT, hit three island groups or affected the Luzon and Mindanao groups (located at the North and South far ends of the country, respectively). Model localization accuracy at a finer level/resolution was not assessed for a twofold reason. Firstly, the model presented here aims to support nationwide parametric programs. The investigated accuracy at island group levels can be deemed appropriate for mobilizing resources towards the affected area faster and overcoming potential bureaucratic bottlenecks associated with resources pre-allocated at different (i.e., finer) administrative levels. Secondly, location information at a finer resolution (city or provincial level) for the investigated historical events was not available.

As mentioned above, the proposed methodology can serve as a basis for the computation of a specific index, upon which the payout of the parametric coverage is based. Such an index could be provided, for instance, as a modeled loss metric (i.e., loss index) computed through an ad-hoc developed vulnerability function relating the event cumulated precipitation with a loss ratio on each active cell. In this way, the loss index would result from the sum of the overall loss computed over a specific event's active cells. The final payout could be directly linked to the loss index within limits defined by the policy regarding the attachment point - minimum loss index value below which the payout is not triggered - and policy limit - maximum payout issued. Alternatively, the index could be based directly on the number of event active cells and/or duration (computed as the number of consecutive aggregation periods where a flood is detected). A payout function can then be defined on such a hazard index; for example, the insured could receive a payout ranging from 20% to 100% of the policy limit as the modeled event characteristics above mentioned (used as proxies of event severity) increase.

Possible improvements in the proposed methodology are the inclusion of a secondary trigger, such as wind, to further minimize basis risk. Another way to improve the model performance could be to mask the active cells with a population density layer to minimize false alarms. Furthermore, more recent and more refined data on satellite precipitation estimates could be used (e.g., the new NASA IMERG (Integrated Multi-satellite Retrievals for GPM) product (Huffman, Bolvin, & Nelkin, 2017), or the MSWEP (Multi-Source Weighted-Ensemble Precipitation) (Beck et al., 2017), which combines several products) to leverage on their enhanced skills and provide more reliable estimates worldwide. These updates will not affect the model structure, but could potentially increase its performance and reduce the basis risk.

Finally, the increasing spread of several types of sensors and the development of satellite technologies with higher revisiting times and resolution will pave the road, in the new future, for new and more accurate data (e.g., rainfall/wind speed

measurements or event flood depth) to be used as a trigger(s) in SPEED-type models, as soon as their temporal coverage will be sufficient to compute meaningful statistics.

6 Code/Data availability

The code was not published in any repository/archive and therefore no DOI is included in the reference list. Data used in this study is: EM-DAT loss events database and CMORPH precipitation data. CMORPH precipitation data is available here: ftp://ftp.cpc.ncep.noaa.gov/precip/CMORPH_V1.0/. The EM-DAT website link is included in the references and access to detailed loss data for the Philippines was granted upon request.

7 Author contribution

Annibale Vecere developed the code both for CMORPH precipitation data processing and model structure definition. He also performed all simulations and tests summarized in the paper. Mario Martina, provided guidance in the development of the methodology and suggestions on model performance verification tests. Ricardo Monteiro and Carmine Galasso provided their supervision in the design of the proposed methodology and in the definition of the case study. Annibale Vecere prepared the manuscript with contributions from all co-authors.

8 References

Albertini, L., & Barrieu, P. (2009). The Handbook of Insurance-Linked Securities, 372. https://doi.org/10.1002/9781119206545

ASEAN, GFDRR, & UNISDR. (2012). Advancing Disaster Risk Financing and Insurance in ASEAN Member States: Framework and Options for Implementation, *2*(April).

Beck, H. E., Vergopolan, N., Pan, M., Levizzani, V., Van Dijk, A. I. J. M., Weedon, G. P., … Wood, E. F. (2017). Global-scale evaluation of 22 precipitation datasets using gauge observations and hydrological modeling. *Hydrology and Earth System Sciences*, *21*(12), 6201–6217. https://doi.org/10.5194/hess-21-6201-2017

Brakenridge, G. Robert. (1993). Dartmouth Flood Observatory (DFO) Space-based: measurement, mapping, and modeling of surface water for research, humanitarian, and water management applications. Retrieved October 8, 2018, from http://floodobservatory.colorado.edu

Brakenridge, G R, Andersona, E., Nghiemb, S. V, Caquard, S., & Shabaneh, T. B. (2003). Flood Warnings , Flood Disaster Assessments , and Flood Hazard Reduction : The Roles of Orbital Remote Sensing. *30th International Symposium on Remote Sensing of Environment*, (Vv), 1–6.

Brakenridge, R., & Anderson, E. (2006). MODIS-based flood detection, mapping and measurement: the potential for

operational hydrological applications. *Transboundary Floods: Reducing Risks through Flood Management*, 1–12.

CCRIF SPC. (2016). The CCRIF Excess Rainfall (XSR) Model, 1–6. Retrieved from http://www.ccrif.org/sites/default/files/publications/CCRIF_Excess_Rainfall_Model_2016_web.pdf

CCRIF SPC. (2018). Caribbean Catastrophe Risk Insurance Facility (CCRIF). Retrieved September 1, 2018, from https://www.ccrif.org/

Chartered Insurance Institute. (2017). Reinsurance glossary. Retrieved September 16, 2019, from https://www.cii.co.uk/learning/knowledge-services/reference-resources/dictionaries/reinsurance-glossary/#

Clarke, A. (2018). Time to Act: Applying the Hours Clause to Hurricane Losses. Retrieved September 29, 2018, from https://www.air-worldwide.com/publications/air-currents/2019/Modeling-Fundamentals--Accounting-for-the-Hours-Clause/

Cummins, J. D., & Mahul, O. (2009). Catastrophe Risk Financing in Developing Countries: Principles for Public Intervention, xxiv, 268. https://doi.org/10.1596/978-0-8213-7736-9

D. Guha-Sapir. (2020). EM-DAT: The Emergency Events Database - Université catholique de Louvain (UCL) - CRED, Brussels, Belgium. Retrieved from www.emdat.be

D'Ayala, D., Galasso, C., Nassirpour, A., Adhikari, R. K., Yamin, L., Fernandez, R., … Oreta, A. (2020). Resilient communities through safer schools. *International Journal of Disaster Risk Reduction*, *45*, 101446. https://doi.org/10.1016/j.ijdrr.2019.101446

Eckstein, D., Künzel, V., Schäfer, L., & Winges, M. (2019). *Global Climate Risk Index 2020*. Retrieved from https://www.germanwatch.org/sites/germanwatch.org/files/20-2-01e Global Climate Risk Index 2020_14.pdf

Figueiredo, R., Martina, M. L. V., Stephenson, D. B., & Youngman, B. D. (2018). A Probabilistic Paradigm for the Parametric Insurance of Natural Hazards. *Risk Analysis*, *38*(11), 2400–2414. https://doi.org/10.1111/risa.13122

Fisher, D. (IFRC), Hagon, K. (IFRC), Lattimer, C., O'Callaghan, S., Swithern, S., & Walmsley, L. (2018). *World Disasters Report 2018. Leaving No One Behind: The International Humanitarian Sector Must Do More to Respond to the Needs of the World's Most Vulnerable People*. Retrieved from www.ifrc.org

Foucart, V. (SCOR G. P. (2013). How parametric re / insurance can support the development of insurability.

Funk, C., Peterson, P., Landsfeld, M., Pedreros, D., Verdin, J., Shukla, S., … Michaelsen, J. (2015). The climate hazards infrared precipitation with stations - A new environmental record for monitoring extremes. *Scientific Data*, *2*, 1–21. https://doi.org/10.1038/sdata.2015.66

Gelaro, R., McCarty, W., Suárez, M. J., Todling, R., Molod, A., Takacs, L., … Zhao, B. (2017). The modern-era retrospective analysis for research and applications, version 2 (MERRA-2). *Journal of Climate*, *30*(14), 5419–5454. https://doi.org/10.1175/JCLI-D-16-0758.1

GFDRR. (2018). *Parametric Indices for Excess Rainfall and Drought Pacific Rapid-Respose Financing*.

Hazell, P., Anderson, J., Balzer, N., Clemmensen, A. H., Hess, U., & Rispoli, F. (2010). The Potential for Scale and Sustainability in Weather Index Insurance for Agriculture and Rural Livelihoods. Retrieved from

http://www.ifad.org/ruralfinance/pub/weather.pdf

Hersbach, H., Bell, B., Berrisford, P., Hirahara, S., Horányi, A., Muñoz-Sabater, J., … Thépaut, J. N. (2020). The ERA5 global reanalysis. *Quarterly Journal of the Royal Meteorological Society*, *146*(730), 1999–2049. https://doi.org/10.1002/qj.3803

Huffman, G., Bolvin, D., & Nelkin, E. J. (2017). Integrated Multi-satellitE Retrievals for GPM (IMERG) Technical Documentation, (March), 1–54. Retrieved from https://pmm.nasa.gov/sites/default/files/document_files/IMERG_technical_doc_3_22_17.pdf

Ibarra, H. (2012). Parametric insurance: general market trends and perspectives for the African insurance sector. Retrieved from http://www.africa-re.com/WEATHERINSURANCE.pdf

Joyce, R. J., Janowiak, J. E., Arkin, P. A., & Xie, P. (2004). CMORPH: A Method that Produces Global Precipitation Estimates from Passive Microwave and Infrared Data at High Spatial and Temporal Resolution. *Journal of Hydrometeorology*, *5*(3), 487–503. https://doi.org/10.1175/1525-7541(2004)005<0487:CAMTPG>2.0.CO;2

Mahul, O., & Skees, J. (2007). *Managing agricultural risk at the country level: The case of index-based livestock insurance in Mongolia*. *World Bank Policy Research Working Paper*.

Mehta, A. (2017). Overview of the Global Disaster Alert & Coordination System (GDACS), 0–10.

Oxfam. (2013). Meso-Level Index Based Flood Insurance, 14–15.

Sevieri, G., Galasso, C., D'Ayala, D., De Jesus, R., Oreta, A., Grio, M. E. D. A., & Ibabao, R. (2020). A multi-hazard risk prioritisation framework for cultural heritage assets. *Natural Hazards and Earth System Sciences*, *20*(5), 1391–1414. https://doi.org/10.5194/nhess-20-1391-2020

Slayback, D. A., Brakenridge, R., & Policelli, F. S. (2012). Near real-time Global Flood Mapping Project. Retrieved October 8, 2018, from https://floodmap.modaps.eosdis.nasa.gov/

Stanimirova, R., Greatrex, H., Diro, R., McCarney, G., Sharoff, J., Mann, B., … Osgood, D. E. (2013). Using Satellites to Make Index Insurance Scalable: Final IRI Report to the ILO Microinsurance Innovation Facility. Retrieved from http://iri.columbia.edu/wp-content/uploads/2014/10/Using-Satellites-Scalable-Index-Insurance-IRI-ILO-report-2013.pdf

Stanski, H. R., Wilson, L. J., & Burrows, W. R. (1989). Survey of common verification methods in meteorology_Part 1_A verification framework. In *World Weather Watch* (Vol. Tech. Rept, pp. 8 pp. (1-8)). Geneva: WMO.

Syroka, J., & Nucifora, A. (2010). National drought insurance for Malawi. *World*, (January). Retrieved from http://papers.ssrn.com/sol3/papers.cfm?abstract_id=1536982

Vecere, A., Martina, M., Monteiro, R., & Galasso, C. (2019). Toward near real-time flood loss estimation : model structure and data requirements. In *Proceedings of ICASP13, May 26-30, 2019, Seoul National University, Seoul, Korea*.

Wald, D. J., Jaiswal, K., Marano, K. D., Bausch, D., & Hearne, M. (2010). PAGER - Rapid Assessment of an Earthquake's Impact. *Fact Sheet 2010-3036*, (September), 1–4.

Wu, H., Adler, R. F., Tian, Y., Huffman, G. J., Li, H., & Wang, J. (2014). Real-time global flood estimation using satellite-

based precipitation and a coupled land surface and routing model. *Water Resources Research*, *50*(3), 2693–2717. https://doi.org/10.1002/2013WR014710